Validity of asymptotic models for water waves

Wooyoung Choi, James M. Hyman & Yi A. Li*
Theoretical Division and Center for Nonlinear Studies
Los Alamos National Laboratory, Los Alamos, NM 87545

July 11, 2001

Abstract

We explore the validity of asymptotic models for water waves by investigating the interactions of finite amplitude solitary waves of the Euler equations and its approximating models: the Korteweg-de Vries, the Boussinesq, and the Green-Naghdi equations. The nonlinear surface wave dynamics governed by the two-dimensional Euler equations is simulated by a new numerical method that solves a system of exact one-dimensional equations reduced from the original system. Traveling wave solutions of this new system are compared with those of the asymptotic models by examining the differences between the speeds, amplitudes and mass of the solitary waves. Both head-on and overtaking collisions of two solitary waves are calculated and analyzed in detail. From our numerical simulations, all the asymptotic models accurately describe the dynamics of small amplitude solitary waves. However, large amplitude waves are much better approximated by the Green-Naghdi equations than the weakly nonlinear asymptotic models.

1 Introduction

We consider the evolution of strongly nonlinear long waves on the free surface in a homogeneous layer of an ideal fluid governed by the two-dimensional Euler equations. We compare numerical solutions of the Euler equations with the much simpler approximate models derived from the original system. The validity of the approximate models is explored by systematically comparing numerical solutions of the Euler equations for solitary waves interactions with those of the approximate models.

*Present address: Dept. of Mathematical Sciences, Stevens Institute of Technology, Hoboken, NJ 07030

Because the full Euler equations are often too complicated to analyze directly, simpler models are commonly used to gain insight into the physical processes governed by these equations (for example, see Choi, 1995). Small-amplitude, long-wavelength waves are approximated by weakly nonlinear long wave models such as the Korteweg-deVries (KdV) and the Boussinesq equations (Korteweg & de Vries 1895; Boussinesq 1877). These equations have led researchers to better understand the physical behaviour of nonlinear waves, and to develop new mathematical theories to explain their behaviour (Scott *et al* 1973). However the weakly nonlinear models are not valid for large amplitude waves for which nonlinear effects become more important. Relaxing the assumption that waves have small amplitude leads to the higher-order nonlinear long wave models such as the Green-Naghdi (GN) equations (Green & Naughdi 1976). Although the GN equations were originally derived using the direct-sheet method, it was shown that they can also be derived directly from the Euler equations by an asymptotic expansion method (Choi & Camassa 1999*a*).

The Fourier and the boundary integral methods are among the most widely used methods to solve the Euler equations. Expressing the wave profile and the velocity potential as the Fourier series in horizontal space, Fenton & Rienecker (1982) combined the fast Fourier transform with the leap-frog scheme for the time evolution to numerically solve the equations. The boundary integral method is based on parameterizing the free surface using the Lagrangian coordinates and, by applying the Green's theorem, the velocity potential is expressed in terms of a distribution of singularities on the free surface. (Longuet-Higgins & Cokelet (1976)). The method has been applied for various discretizations of the singular integrals that must be approximated.

Here we solve a system of pseudo-differential evolution equations reduced from the Euler equations for the free surface elevation and the velocity potential on the parameterized free surface. This system was first derived by Dyachenko, Zakharov & Kuznetsov (1996) by using the time-dependent conformal mapping of the fluid region of interest to a strip. This idea was further developed and tested by Choi & Camassa (1999*b*) for periodic traveling waves. The new formulation provides a novel way of computing the evolution of

fully nonlinear surface waves without solving the two-dimensional Euler equations. Unlike the boundary integral method, the new formulation does not require approximating complicated singular integrals and is easily approximated by the discrete Fourier transformation.

After describing our numerical method for solving the new exact evolution equations, we review the derivation of the KdV, the Boussinesq, and the GN equations, and describe the relationships between them. We then compare our numerical solutions for solitary waves with those for the approximate models. Finally, we study solitary wave collisions and discuss the differences between the waves following the collision.

2 Exact evolution equations

A two-dimensional ideal flow between the free surface at $y = \zeta(x,t)$ and a flat bottom at $y = -h$ is governed by the Euler equations. These equations can be expressed in terms of the velocity potential $\Phi(x,y,t)$ as

$$\begin{array}{ll} \Phi_{xx} + \Phi_{yy} = 0, & -h < y < \zeta,\ -\infty < x < \infty, \\ \Phi_y = \zeta_t + \Phi_x \zeta_x, & -\infty < x < \infty,\ y = \zeta(x,t), \\ \Phi_t + \frac{1}{2}|\nabla\Phi|^2 + gy = \mathcal{S} + \mathcal{P}_E/\rho, & -\infty < x < \infty,\ y = \zeta(x,t), \\ \Phi_y = 0, & -\infty < x < \infty,\ y = -h. \end{array} \tag{2.1}$$

Here ρ is the fluid density, $\mathcal{S} = \sigma\zeta_{xx}/(1+\zeta_x^2)^{3/2}$ is the surface tension, and $\mathcal{P}_E(x,t)$ is a prescribed external atmospheric pressure.

Following the work by Dyachenko *et al* (1996) and Choi & Camassa (1999*b*), let $z(\xi,\eta,t) = x(\xi,\eta,t) + iy(\xi,\eta,t)$ be an analytic function in the horizontal strip $-\bar{h} \le \eta \le 0$, where $z - \xi$ is periodic in ξ with the period l, such that z maps the rectangle of $-l/2 \le \xi \le l/2$, $-\bar{h} \le \eta \le 0$ onto the fluid domain. The mapping function satisfies $y(\xi,0,t) = \zeta(x(\xi,0,t),t)$ and $y(\xi,-\bar{h},t) = -h$ for any $\xi \in [-l/2, l/2]$.

It follows from the Cauchy-Riemann equations that the parameterized functions $x(\xi,\eta,t)$, $y(\xi,\eta,t)$, $\phi(\xi,\eta,t) = \Phi(x(\xi,\eta,t),y(\xi,\eta,t),t)$ and its harmonic conjugate $\psi(\xi,\eta,t)$ are related by Fourier multiplier transforms (Choi & Camassa 1999*b*). That is, if the Fourier

series of $y(\xi,0,t)$ and $\psi(\xi,0,t)$ are given by

$$y(\xi,0,t) = a_0 + \sum_{k=1}^{\infty}\big[a_k\cos(2\pi k\xi/l) + b_k\sin(2\pi k\xi/l)\big],$$
$$\psi(\xi,0,t) = \alpha_0 + \sum_{k=1}^{\infty}\big[\alpha_k\cos(2\pi k\xi/l) + \beta_k\sin(2\pi k\xi/l)\big],$$

then, for any $\eta \in [-\bar{h},0]$, the following relations hold

$$\begin{aligned}
y(\xi,\eta,t) &= \frac{a_0+h}{\bar{h}}\eta + a_0 + \sum_{k=1}^{\infty} S_h\big[a_k\cos(2\pi k\xi/l) + b_k\sin(2\pi k\xi/l)\big],\\
\psi(\xi,\eta,t) &= \frac{\alpha_0}{\bar{h}}\eta + \alpha_0 + \sum_{k=1}^{\infty} S_h\big[\alpha_k\cos(2\pi k\xi/l) + \beta_k\sin(2\pi k\xi/l)\big],\\
x(\xi,\eta,t) &= \frac{a_0+h}{\bar{h}}\xi + x_0 + \sum_{k=1}^{\infty} C_h\big[a_k\sin(2\pi k\xi/l) - b_k\cos(2\pi k\xi/l)\big],\\
\phi(\xi,\eta,t) &= \frac{\alpha_0}{\bar{h}}\xi + \phi_0 + \sum_{k=1}^{\infty} C_h\big[\alpha_k\sin(2\pi k\xi/l) - \beta_k\cos(2\pi k\xi/l)\big],
\end{aligned} \tag{2.2}$$

where

$$S_h = \sinh\big[2\pi k\big(\eta+\bar{h}\big)/l\big]/\sinh\big(2\pi k\bar{h}/l\big),$$
$$C_h = \cosh\big[2\pi k\big(\eta+\bar{h}\big)/l\big]/\sinh\big(2\pi k\bar{h}/l\big).$$

The time derivatives in (2.2) are periodic in ξ if the coefficients for the leading linear terms with respect to η and ξ are constants. This is accomplished by choosing $\bar{h}$ and α_0 as $\bar{h}(t)$=$a_0(t) + h$ and $\alpha_0(t)$=$c\bar{h}(t)$, where the constant c is determined from the initial condition.

On the free surface at $\eta = 0$, the following relations follow from (2.2):

$$x_\xi = 1 + Ty_\xi\,, \qquad \phi_\xi = c + T\psi_\xi\,.$$

Therefore,

$$x = \xi + x_0 + Ty\,, \qquad \phi = c\xi + \phi_0 + T\psi\,,$$

where x_0 and ϕ_0 are functions of time to be determined. T is the Fourier multiplier operator defined by

$$T[y] \stackrel{\text{def}}{=} \sum_{k=1}^{\infty} \coth(2\pi k\bar{h}/l) \left[a_k \sin(2\pi k\xi/l) - b_k \cos(2\pi k\xi/l)\right], \tag{2.3}$$

which we call the Tilbert or T-transform. For deep water ($h \to \infty$), this becomes the Hilbert transformation.

By substituting the expressions for x, y, ϕ and ψ at $\eta = 0$ into the boundary conditions at the free surface in (2.1), we obtain the *surface Euler equations*

$$\begin{aligned} x_t &= -x_\xi T\left[\frac{\psi_\xi}{J}\right] + y_\xi \left(\frac{\psi_\xi}{J}\right), \\ y_t &= -x_\xi \left(\frac{\psi_\xi}{J}\right) - y_\xi T\left[\frac{\psi_\xi}{J}\right], \\ \phi_t &+ \phi_\xi T\left[\frac{\psi_\xi}{J}\right] + \frac{1}{2J}\left(\phi_\xi^2 - \psi_\xi^2\right) + gy = \mathcal{S} - \mathcal{P}_E/\rho, \end{aligned} \tag{2.4}$$

where $J = x_\xi^2 + y_\xi^2$ and $\mathcal{S} = \sigma(y_{\xi\xi}x_\xi - y_\xi x_{\xi\xi})/J^{3/2}$ is the surface tension.

Equations (2.4) are the exact parametric evolution equations for surface waves in water of finite depth, governed by the Euler equations (2.1). Since x and y are related by the Cauchy-Riemann equations, it is sufficient to solve one of the first two equations with the third equation in (2.4). Even so, we found it convenient to numerically solve all these equations and determine both $x_0(t)$ and $a_0(t)$ from the first two equations.

At each time step, the periodic functions in (x, y, ϕ, ψ) are expanded as the discrete Fourier series with respect to the variable ξ and we use the fast Fourier transform (Staley 1999) to compute their derivatives and the T-transform. We advance the solution of (2.4) in time with a variable-order, variable-stepsize, Adams-Bashford-Moulton predictor-corrector method (see Schiesser, 1993).

In the absence of surface tension and atmospheric external pressure, the surface wave equations have nine one-parameter symmetry groups (Benjamin and Olver 1982), from which eight conserved quantities can be found. The accuracy of our numerical solutions

was monitored by the following three conserved quantities: conservation of mass

$$\int_{-l/2}^{l/2} y(\xi) x_\xi(\xi)\, d\xi,$$

conservation of the horizontal momentum

$$\int_{-l/2}^{l/2} \phi_\xi(\xi) y(\xi)\, d\xi\,,$$

and conservation of energy

$$\int_{-l/2}^{l/2} \big(\phi_\xi(\xi)\psi(\xi) + g y(\xi)^2 x_\xi(\xi)\big)\, d\xi.$$

Here the conserved quantities are expressed using the parameterized formulation defined in the interval $[-l/2, l/2]$. The numerical error tolerance was set between 10^{-9} and 10^{-12} per unit time depending on the length of time for the calculations. The spatial resolution was between 512 and 2048 Fourier mode based the steepness of the solution. The time step and spatial resolution was determined so that the absolute error of the conserved quantities was below 10^{-4} and the relative error was below 10^{-3}.

We used artificial dissipation (hyperviscosity) to reduce the aliasing due to the nonlinear terms and the numerical errors in solving (2.4). The diffusive terms $\nu \triangle\xi\, x_{\xi\xi}$, $\nu \triangle\xi\, y_{\xi\xi}$ and $\nu \triangle\xi\, \phi_{\xi\xi}$ were passed through a high pass filter and were added to the right-hand side of the x, y, and ϕ equations, respectively. Here $\triangle\xi$ is the spatial step size and ν was chosen in the range between 0.01 and 0.05. To preserve the accuracy in the lower frequency modes, we also applied a high pass filter defined in the Fourier space to these artificial dissipation terms. The filter eliminated the lowest 1/2 Fourier modes of the dissipation terms, left the highest 3/5 modes unchanged, and had a linear transition between the two regions. Thus, the dissipation had no direct effect on the lower 1/2 of the Fourier modes of the solution, and only dissipated the higher modes.

3 Approximate model equations

Here we briefly sketch their derivation of the KdV, Boussinesq and GN equations modeling nonlinear long waves in shallow water. The derivations all assume the typical wavelength

l is much greater than the water depth h.

By substituting $x = lX$, $y = h(Y-1)$, $t = lT/c_0$, $\zeta = h(H-1)$, $\Phi = c_0 l\varphi + c_0^2 t$ and $c_0^2 = gh$ into the surface Euler equations for water waves (2.1) with $\mathcal{S} = \mathcal{P}_E = 0$, we obtain the dimensionless equations

$$\begin{array}{ll} \epsilon^2\varphi_{XX} + \varphi_{YY} = 0, & 0 < Y < H, \\ \epsilon^2\varphi_T + \frac{1}{2}(\epsilon^2\varphi_X^2 + \varphi_Y^2) + \epsilon^2 H = 0, & Y = H, \\ \epsilon^2 H_T + \epsilon^2 H_X\varphi_X = \varphi_Y, & Y = H, \\ \varphi_Y = 0, & Y = 0\,, \end{array} \tag{3.1}$$

where $\epsilon = h/l \ll 1$ for long waves.

The velocity potential φ, satisfying the Laplace equation and the bottom boundary condition at $Y = 0$, can be expressed by

$$\varphi(X,Y,T) = \sum_{k=0}^{\infty} \frac{(-1)^k \epsilon^{2k} Y^{2k}}{(2k)!} \frac{\partial^{2k} f(X,T)}{\partial X^{2k}}\,. \tag{3.2}$$

Substituting this expansion into the free surface boundary conditions at $Y = H$ in (3.1) yields the equations for H and $w \equiv f_X$

$$\begin{aligned} H_T + (Hw)_X &= \frac{\epsilon^2}{6}(H^3 w_{XX})_X + O(\epsilon^4), \\ w_T + ww_X + H_X &= \frac{\epsilon^2}{3}\Big[H^2(w_{XT} + ww_{XX} - w_X^2)\Big]_X + O(\epsilon^4)\,. \end{aligned} \tag{3.3}$$

Since $\varphi_X = w - \epsilon^2 Y^2 w_{XX}/2 + O(\epsilon^4)$ from (3.2), the depth-mean horizontal velocity u can be expressed as

$$u = \frac{1}{H}\int_0^H \varphi_X dY = w - \frac{\epsilon^2 H^2}{6} w_{XX} + O(\epsilon^4)\,. \tag{3.4}$$

This equality can be used to express w, in term of u, as

$$w = u + \frac{\epsilon^2 H^2}{6} u_{XX} + O(\epsilon^4).$$

The system (3.3) can now be rewritten in terms of H and u to give the GN equations

$$\begin{aligned} H_T + (Hu)_X &= 0, \\ u_T + uu_X + H_X &= \frac{\epsilon^2}{3H}\Big[H^3\big(u_{XT} + uu_{XX} - u_X^2\big)\Big]_X + O(\epsilon^4)\,. \end{aligned} \tag{3.5}$$

This asymptotic expansion derivation of the GN equations is analogous to the approach Whitham (1974) used to derive the Boussinesq equations. The system (3.5) was originally derived by Green & Naghdi (1976) using the 'direct-sheet' theory. An alternative derivation can also be found in Choi & Camassa (1999*a*).

Notice that the first equation in (3.5) is exact, while the second equation for the conservation of momentum contains an error of $O(\epsilon^4)$. Because we have not assumed that the wave amplitudes are small, the GN equations should be a good approximation of the Euler equations, even for large amplitude waves, as long as the long-wave approximation ($\epsilon \ll 1$) is valid.

Using the horizontal velocity defined at a certain depth, instead of the depth mean velocity u in (3.5), results in other forms of equations, for example, the system by Wei *et al* (1995). These other models are all asymptotically equivalent to (3.5).

Substituting $H = 1 + \alpha\tilde{\zeta}$ and $u = \alpha\tilde{u}$ for $\alpha = a/h$ into the GN equations (3.5) and dropping $O(\alpha\epsilon^2)$ for weakly nonlinear waves lead to the Boussinesq equations:

$$\begin{aligned} &\tilde{\zeta}_T + \Big[(1+\alpha\tilde{\zeta})\tilde{u}\Big]_X = 0, \\ &\tilde{u}_T + \alpha\tilde{u}\tilde{u}_X + \tilde{\zeta}_X = \frac{\epsilon^2}{3}\tilde{u}_{XXT}. \end{aligned} \tag{3.6}$$

The KdV equation can be derived from the Boussinesq system (3.6) by assuming the waves all travel in the same direction (*e.g.* see Whitham, 1974).

The *GN equations* (3.5) in dimensional variables are

$$\begin{aligned} &\eta_t + (u\eta)_x = 0, \qquad \eta = h + \zeta\,, \\ &u_t + uu_x + g\eta_x = \frac{1}{3\eta}\left[\eta^2\frac{d}{dt}(\eta u_x)\right]_x, \end{aligned} \tag{3.7}$$

where we have used $d(\eta u_x)/dt = (\eta u_x)_t + u(\eta u_x)_x$.

In dimensional variables, the *Boussinesq equations* (3.6) are

$$\begin{aligned} &\zeta_t + \Big[(h+\zeta)u\Big]_x = 0, \\ &u_t + uu_x + g\,\zeta_x = \frac{h^2}{3}\,u_{xxt}\,, \end{aligned} \tag{3.8}$$

and the *KdV equation* is

$$\zeta_t + c_0\,\zeta_x + \frac{3c_0}{2h}\,\zeta\zeta_x + \frac{c_0 h^2}{6}\,\zeta_{xxx} = 0\,, \tag{3.9}$$

where $c_0 = \sqrt{gh}$.

4 Solitary wave solutions

The solitary travelling wave solutions for the KdV and GN equations are given by

$$\zeta_{KdV} = \frac{2h(c-c_0)}{c_0}\,\mathrm{sech}^2\,\frac{\sqrt{3(c-c_0)}\,(x-ct)}{\sqrt{2c_0}\,h},$$

$$\zeta_{GN} = \frac{c^2-c_0^2}{g}\,\mathrm{sech}^2\,\frac{\sqrt{3(c^2-c_0^2)}\,(x-ct)}{2ch},$$

respectively, for given wave speed c. The explicit solitary wave solutions for the Euler and Boussinesq equations are not known, and we calculated them numerically in our comparisons.

4.1 Numerical methods

By using the KdV scaling, Friedrichs & Hyers (1954) and Beale (1977) proved the existence of solitary waves for the Euler equations in the weakly nonlinear regime where the Froude number $F = c/\sqrt{gh}$ is greater than but close to one. They also showed that the KdV solitary waves approximate those of the Euler equations. Amick & Toland (1981) showed the existence of solitary waves for the Euler equations as the limit of periodic waves even beyond the weakly nonlinear regime. Based on their results, we approximated the solitary waves of the Euler equations by long wavelength periodic waves.

We look for travelling waves of the form

$$x = \xi + \tilde{x}(\xi - ct), \quad y = y(\xi - ct), \quad \phi = \delta(\xi - ct) + \tilde{\phi}(\xi - ct), \quad \psi = \psi(\xi - ct),$$

where $\tilde{x}(= Ty)$, y, ψ and $\tilde{\phi}$ are periodic functions of $s = \xi - ct$ with the period l and δ which are constants to be determined. The functions y and $\tilde{\phi}$ satisfy the boundary

conditions $y\big(l/2\big) = \tilde{\phi}_\xi\big(l/2\big) + \delta = 0$, and y is even and symmetric with respect to $s = 0$. As $l \to \infty$, $y(s)$ converges to a solitary wave decaying to zero (Amick & Toland 1981).

Substituting the travelling wave into the kinematic equation $y_t x_\xi - x_t y_\xi = -\psi_\xi$ (Choi & Camassa 1999*b*), we obtain $cy_s = \psi_s$. Because $\tilde{x}$ and ϕ are harmonic conjugates of y and ψ, respectively, we have that $\phi_s(s) = c\big(\tilde{x}_s(s) - \tilde{x}_s\big(l/2\big)\big)$, *i.e.* $\delta = -c\tilde{x}_s\big(l/2\big)$. Substituting these relations into the third equation of (2.4) and assuming that the surface tension $\mathcal{S}$ and the external pressure $\mathcal{P}_E$ are negligible, we obtain the free surface equation at $\eta = 0$

$$x_\xi^2 + y_\xi^2 = \frac{x_s^2\big(l/2\big)}{1 - 2gy/c^2}\,.$$

Substituting $s = \bar{h}\xi$, $x = \bar{h}\hat{x}$, $\eta = \bar{h}\hat{\eta}$ and $y = \bar{h}\hat{y}$ into this equation leads to the dimensionless free surface equation

$$\hat{x}_\xi^2 + \hat{y}_\xi^2 = \frac{\hat{x}_\xi^2\big(l/2\big)}{1 - 2g\bar{h}\hat{y}/c^2} \quad \text{at } \eta = 0\,. \tag{4.1}$$

Because the Euler equations have a one-parameter scaling symmetry group $(\lambda x, \lambda y, \lambda^{\frac{1}{2}} t, \lambda^{\frac{3}{2}}\phi)$ (Benjamin & Olver 1982) for any $\lambda > 0$, without loss of generality, we set $\bar{h} = 1$ in the following analysis. Also, for simplicity, we will drop the accent $\hat{}$ over x and y.

Let w and θ be real-valued functions such that $z_\xi = x_\xi + iy_\xi = e^{w+i\theta}$. Because z_ξ is an analytic function of $\xi + i\eta$, w and θ satisfy the Cauchy-Riemann equations. Using the KdV scaling (Friedrichs & Hyers 1954), $\xi^* = a\xi$, $\theta^* = a^{-3}\theta$ and $w^* = a^{-2}w$, the equation for the free surface given by (4.1) can be expressed as

$$w_\xi = \frac{1}{a^3} e^{a^2\left(3w - 2w(l/2) - 1\right)} \sin a^3\theta \quad \text{at } \eta = 0\,, \tag{4.2}$$

where $e^{a^2} = c^2/\big(g\bar{h}\big)$ and we have dropped the asterisks for simplicity.

The exponent in (4.2) can be found using the Cauchy-Riemann relations as

$$3w - 2w(l/2) = 3T_a[\theta] - 2T_a[\theta(l/2)] + < w > \equiv M_a[\theta]\,, \tag{4.3}$$

where $T_a[\theta]$ is the scaled complex T-transform (2.3),

$$T_a[\theta] = -ia \sum_{k \neq 0} \coth(2\pi ak/l)\, c_k e^{2\pi ik\xi/l}\,.$$

Here $< w >$ is the average value of w over one period,

$$< w >= -\frac{1}{a^2} \log \left[\frac{1}{l} \int_0^l e^{a^2 T_a \theta} \cos(a^3 \theta) d\xi \right] .$$

By using (4.3), equation (4.2) can be written as

$$f[\theta] \equiv \theta - (G[\theta] - I)^{-1} \left[\frac{1}{a^3} e^{a^2 \left(M_a[\theta] - 1 \right)} \sin(a^3 \theta) - \theta \right] = 0 , \tag{4.4}$$

where

$$G[\theta] \stackrel{\text{def}}{=} a \sum_{k \neq 0} kl \coth(2\pi a k / l) \, c_k e^{2\pi i k \xi / l} .$$

To solve (4.4) with the Newton's method, we express the $(n+1)$st approximation to θ as $\theta_{n+1} = \theta_n + v_n$, where θ_n is the approximation from the previous iteration and v_n is the correction. We then linearize (4.4) with respect to v_n to obtain $f_{\theta_n}[v_n] = -f[\theta_n]$. Here f_θ is the functional derivative of f with respect to θ

$$f_{\theta_n}[v_n] \equiv v_n - (G - I)^{-1} \left[\frac{1}{a} e^{a^2 \left(M_a[\theta_n] - 1 \right)} \sin(a^3 \theta_n) \frac{\delta M_a}{\delta \theta_n} + e^{a^2 \left(M_a[\theta_n] - 1 \right)} \cos(a^3 \theta_n) - 1 \right] v_n .$$

After we compute f_θ, we define the $N \times N$ matrix, F_θ, as f_θ modulus its kernel using the discrete Fourier Transform for N Fourier modes. We then solve $F_{\theta_n}[v_n] = -f[\theta_n]$ for v_n and iterate until $|v_n| < 10^{-13}$.

Because the small amplitude travelling waves of the KdV equation are close approximations to those of the Euler equations (Friedrichs & Hyers 1954; Beale 1977), in the weakly nonlinear regime (small $a > 0$), we use the KdV travelling waves as the initial guess to find traveling wave solutions of (4.2). We then gradually increase the parameter a (thus, increasing the speed c), and use solutions for the smaller waves as an initial guess to compute higher amplitude waves as the solution of a fixed point problem. In the weakly nonlinear regime, if we increase a by 7%, it takes only six iterations for this scheme to reduce the error to $\sup |\theta_{n+1} - \theta_n| < 10^{-13}$ and $\sup |f[\theta_n]| < 10^{-13}$.

Using this numerical method, we are able to solve for solitary waves of the surface Euler equations with the Froude number up to $F = 1.27$ using 2048 discrete Fourier modes. Beyond $F = 1.27$, the steepening slope of the solitary waves requires more Fourier

modes to reduce numerical errors. Because our objective is to investigate the differences between the model equations and not to compute the highest solitary wave, which is known to have the discontinuity of wave slope near $F \approxeq 1.286$, we limited $F < 1.27$.

4.2 Numerical results

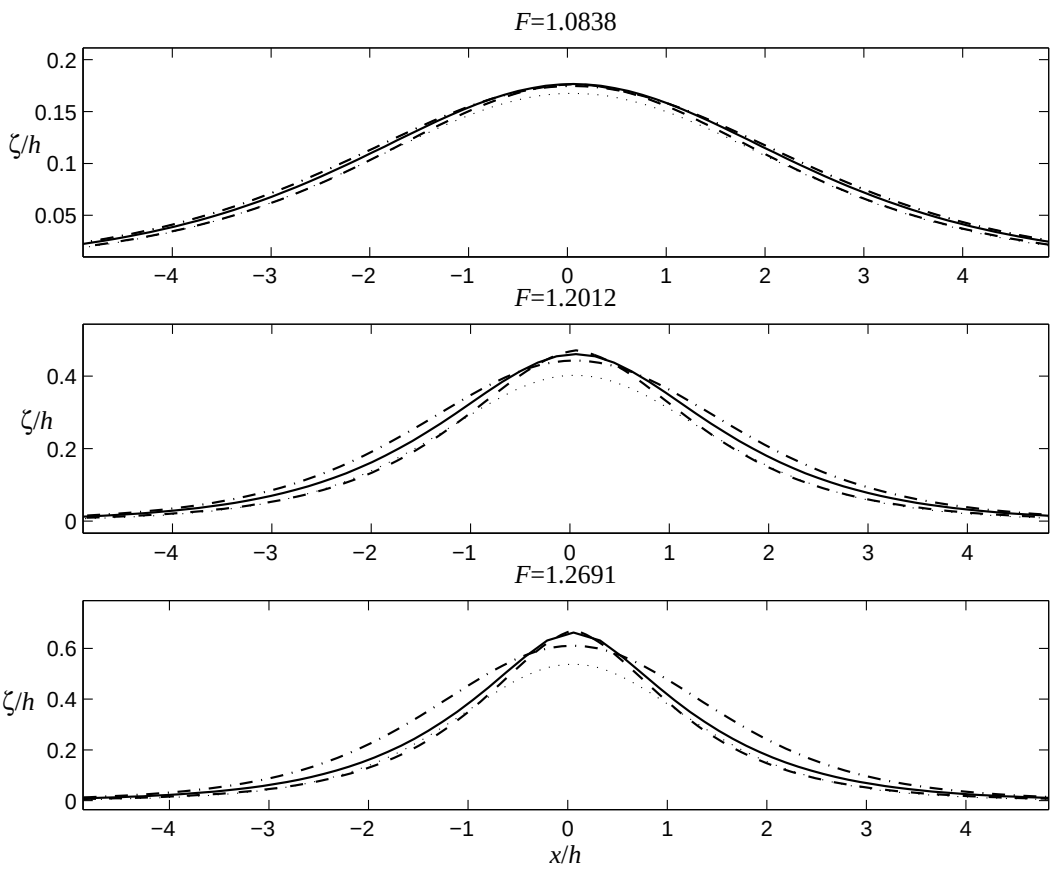

Figure 1: Solitary wave profiles at the Froude numbers of F =1.0838, 1.2012 and 1.2691 for the Euler (solid curve), GN (dash-dotted curve), Boussinesq (dashed curve), and KdV (dotted curve) equations.

In Fig. 1, we compare the wave profiles of the models for three Froude numbers $F = c/\sqrt{gh}$ =1.0838, 1.2012, 1.2691. When $1 < F \leq 1.1$, solitary wave solutions of the KdV, Boussinesq and GN Equations are very close to those of the Euler equations, as expected. However, as F increases, the solitary waves of the KdV equation deviate from those of the Euler equations. In particular, as F increases, the KdV solitary wave is much lower

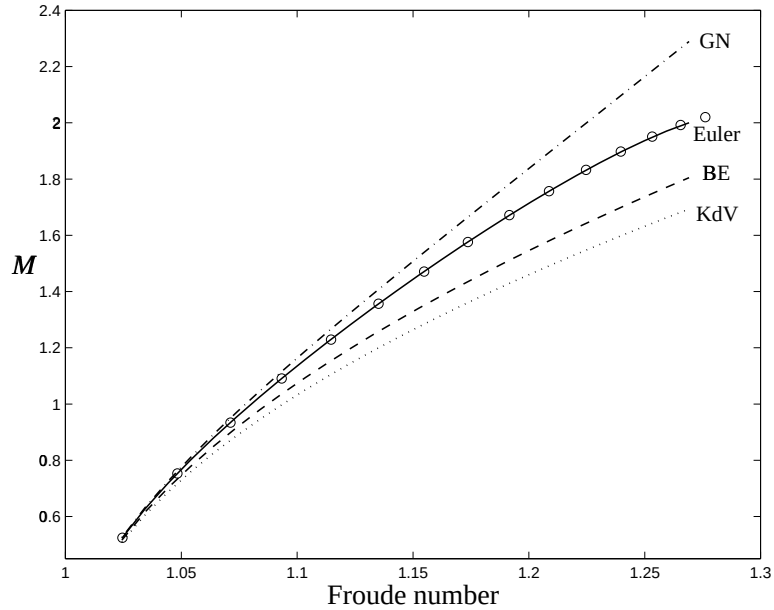

Figure 2: The solitary waves increases in height and mass M as a function of the Froude number F for the Euler (solid curve), GN (dash-dotted curve), Boussinesq (dashed curve), KdV (dotted curve) and Longuet-Higgins & Fenton (circle) models. The mass of the full Euler equation travelling waves calculated by Longuet-Higgins asymptotic expansion method is in excellent agreement with the solitary waves for our surface Euler equation model (2.4). The GN equations show better agreement with the Euler equations than the weakly nonlinear models for intermediate wave amplitude waves.

than the Euler solitary wave. This also implies that the KdV waves are faster than Euler waves of the same height. The solitary wave profile for the GN and Boussinesq equations are slightly above and below the Euler solitary wave, respectively, but much closer to the correct amplitude than the KdV wave.

It is difficult to tell which of these two models is better by just comparing wave profiles. At $F = 1.2691$, the Boussinesq solitary wave profile is closer to the Euler equations in terms of its width. For high Froude numbers, the GN solitary waves are wider than those of the Euler equations.

In Figs. 2 and 3, we compare the scaled mass of solitary waves $M = \int_{\mathbb{R}} \eta dx/h^2$ and the scaled wave amplitude a/h as a function of the Froude number. The figures also confirm that the solitary waves for (2.4) agree with the solutions of the Euler equations (as calculated by Longuet-Higgins (1974) and Longuet-Higgins & Fenton (1974)) to within

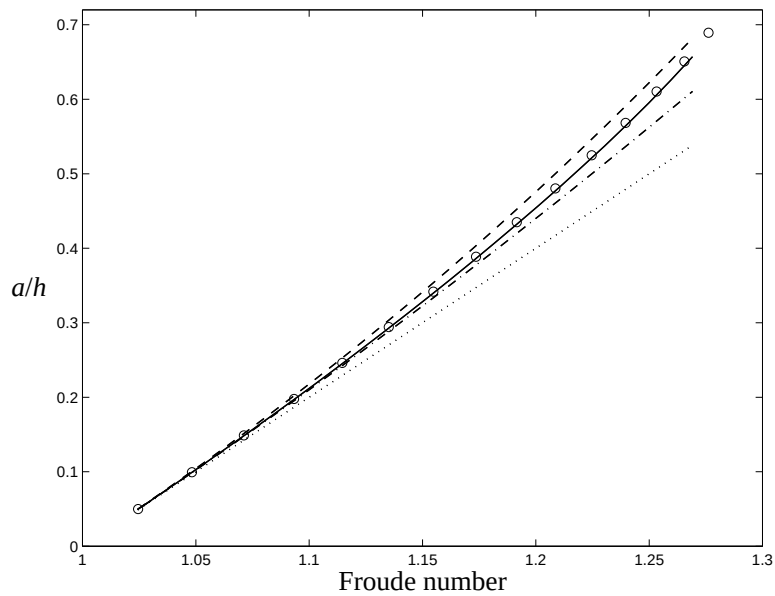

Figure 3: Froude number F versus wave amplitude a/h; Euler (solid curve), GN (dash-dotted curve), Boussinesq (dashed curve), KdV (dotted curve) and Longuet-Higgins & Fenton (circle). Notice that the KdV solitary wave of given wave amplitude is moving much faster than the surface Euler equations wave with the same amplitude.

0.16% for M and 0.35% for a/h.

When the Froude number is close to 1 ($1 \leq F < 1.1$), all the solitary waves have almost the same mass (Fig. 2). As F increases ($1.1 < F < 1.2$), the mass of the solitary waves of the weakly nonlinear KdV and Boussinesq equations are less than the Euler solitary waves. For $F < 1.2$, the solitary wave mass of the strongly nonlinear long wave model (GN) is closer to the Euler wave than the other models. When $F > 1.2$, none of the approximate models are accurate.

Because the derivation for the GN equations did not assume that the wave amplitude is small, it is not surprising that the GN equations are valid at larger F than the other models. The GN equations fail completely as the Froude number approaches the maximum $F = 1.286$ (Longuet-Higgins & Fentons 1974). As F approaches 1.286, the sides of the solitary wave wave steepen until the slope is discontinuous. Beyond $F = 1.286$, none of the long wave shallow water models are valid. The formation of the singularity may explain why the GN solitary waves differ from the Euler solitary waves for $F > 1.2$.

Choi & Camassa (1999*a*) studied the coupled GN equations for strongly nonlinear long waves at the interface between two fluids. As the internal solitary wave amplitude approaches its maximum value, instead of the slope becoming discontinuous, the wave becomes a front varying smoothly from one level to another. Therefore, unlike the GN equations for surface gravity waves, the GN equations for internal gravity waves are valid even for very large solitary waves.

The solitary wave amplitude of the KdV equation is much smaller than the wave of the Euler equations at the same Froude number (Fig. 3). The weakly nonlinear Boussinesq model is much better than the KdV equation but it still over-predicts wave amplitude for the whole range of Froude number. The GN equations well predict the wave amplitude for $F < 1.2$.

In conclusion, based on the comparison of the solitary wave solutions, the GN equations show better agreement with the Euler equations than the weakly nonlinear models.

5 Collision of two solitary waves

We now investigate the differences of dynamical behaviours between the models by studying head-on and overtaking solitary wave collisions. Throughout this section, time t is non-dimensionalized by h/c_0.

5.1 Head-on collision

In the head-on collisions, shown in Fig. 4, solitary waves with $F = 1.172$ and $F = 1.084$ propagating in the opposite directions collide and emerge with oscillating tails. We matched the wave speeds for the different models, and thus wave amplitudes are different as discussed in §4.2. Initially, the amplitudes of the larger waves are $A_E/h = 0.3847$, $A_G/h = 0.3727$ and $A_B/h = 0.3991$ and those of the smaller waves are $a_e/h = 0.1765$, $a_g/h = 0.1744$ and $a_b/h = 0.1801$ for the Euler, GN and Boussinesq equations, respectively. Because the KdV waves are unidirectional, the model was not included in this example. Notice that the amplitudes of the larger waves are not in the weakly nonlinear

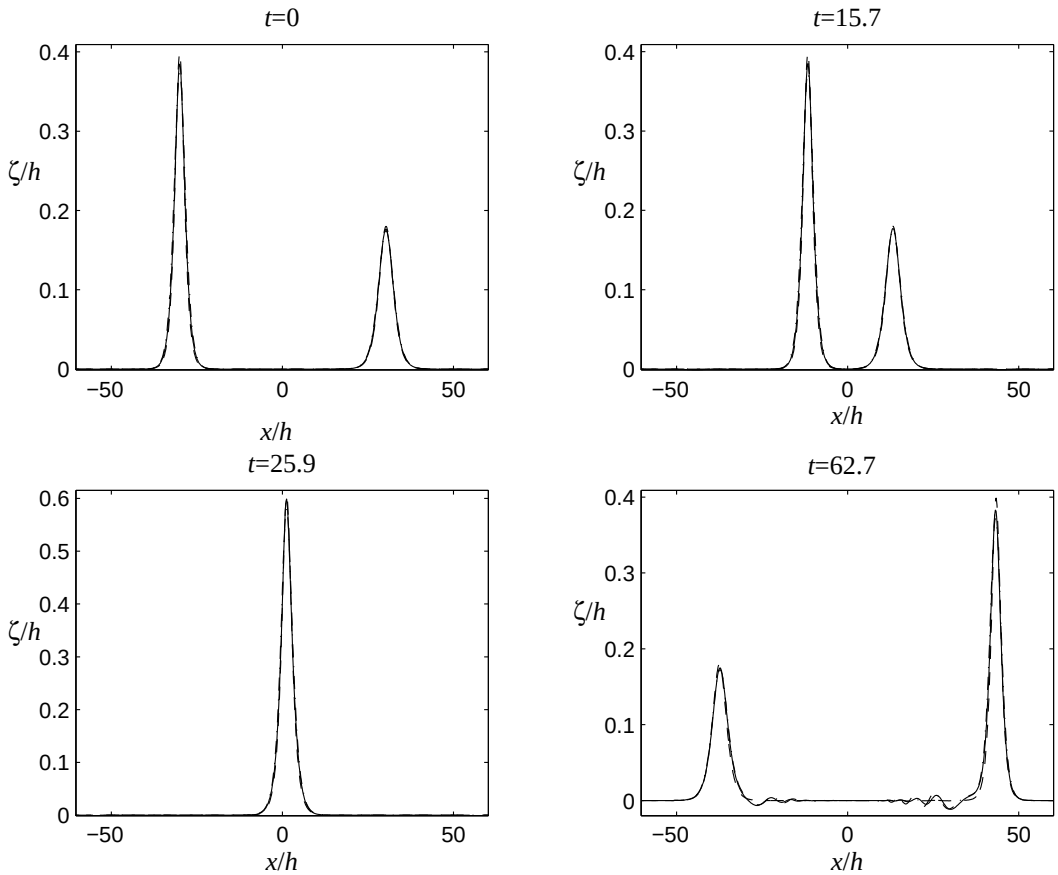

Figure 4: The head-on collision of two solitary waves of the Euler equations (solid curve) is compared to the solutions of the GN equations (dash-dotted curve) and the Boussinesq equations (dashed curve), respectively, with the Froude numbers of $F = 1.084$ and $F = 1.172$. At $t = 25.9$, the two solitary waves have merged into a single pulse with height greater than the sum of the amplitude of the two original waves.

regime.

As shown in Fig. 4, two solitary waves collide and merge to form a single peak at $t = 25.9$ with amplitudes of $A_E/h = 0.5991$, $A_G/h = 0.5802$ and $A_B/h = 0.6052$. The height of the peak during the collision is always greater than the sum of two wave amplitudes. After colliding, all the waves shed dispersive waves behind them and the amplitudes of both waves slightly decrease. At $t = 62.7$, the larger waves have amplitudes of $A_E/h = 0.3828$, $A_G/h = 0.3717$ and $A_B/h = 0.3989$, the smaller waves have amplitudes of $a_e/h = 0.1748$, $a_g/h = 0.1725$ and $a_b/h = 0.1800$.

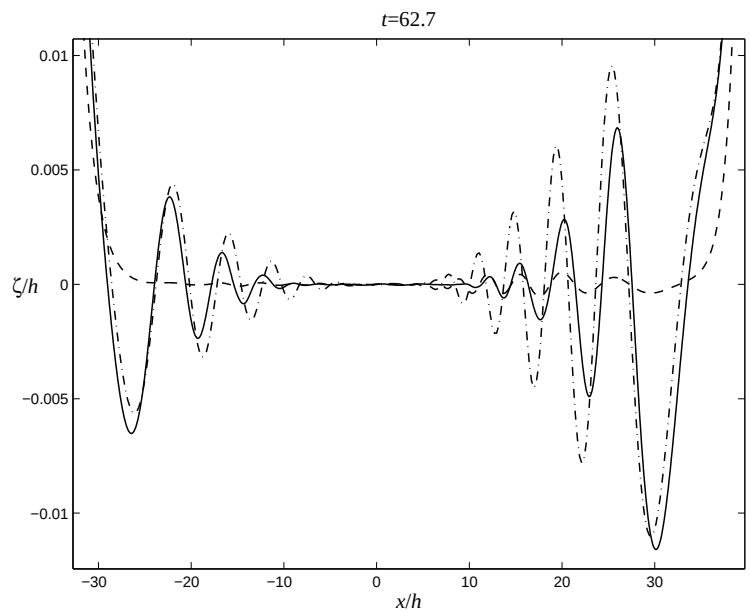

Figure 5: The trailing tails of the solitary waves after the head-on collision shown in Fig. 4 at $t = 62.7$ for the Euler (solid curve), GN (dash-dotted curve) and Boussinesq (dashed curve) equations. Notice that the GN wave tails is much closer to the Euler solution.

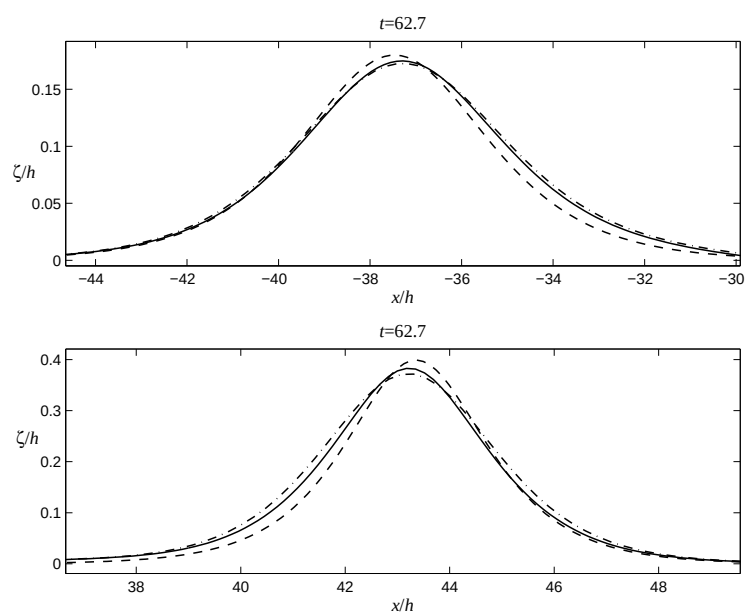

Figure 6: The final wave profiles for $F = 1.084$ and $F = 1.172$ after the head-on collision shown in Fig. 4 for the Euler (solid curve), GN (dash-dotted curve) and Boussinesq (dashed curve) equations. The GN solitary waves are in phase with the Euler solitary waves, while the Boussinesq equations underpredict the phase shift.

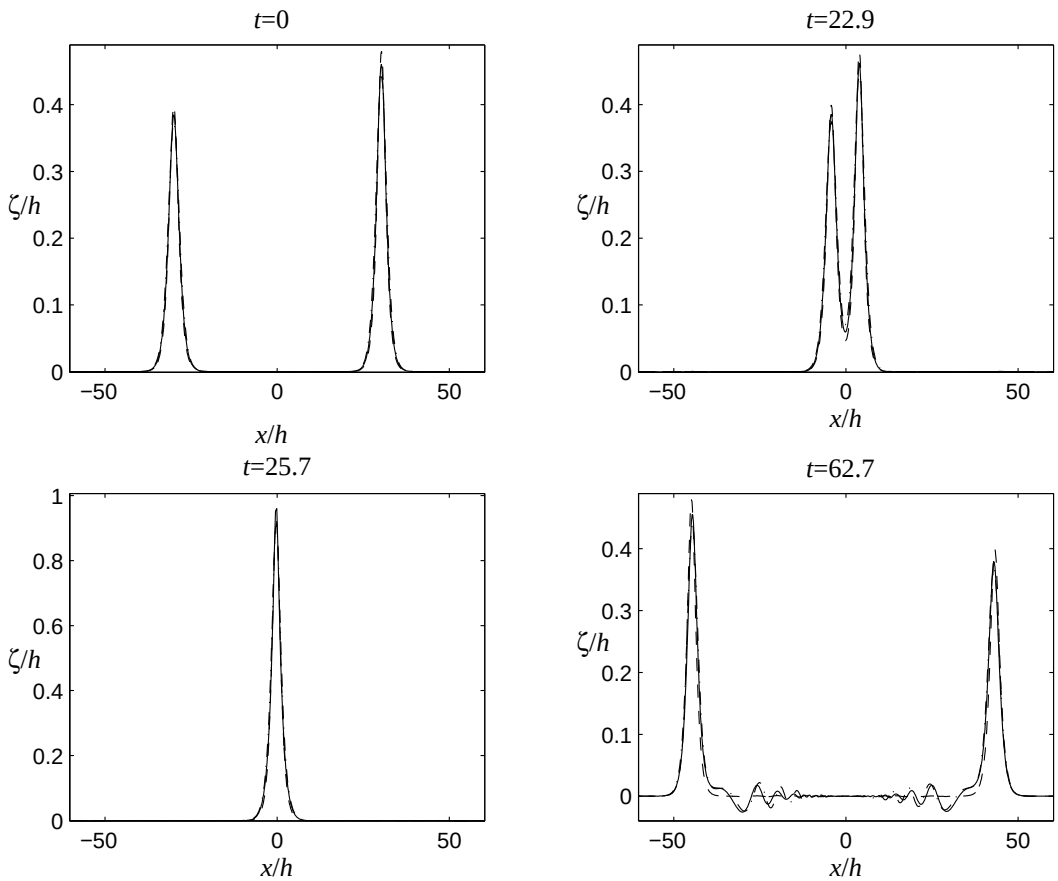

Figure 7: The head-on collision of two solitary waves of the Euler (solid curve), the GN (dash-dotted curve) and Boussinesq equations (dashed curve), respectively, with the Froude numbers $F = 1.172$ and $F = 1.201$. Notice that the trailing edge of the Boussinesq waves is a poor approximation to the Euler wave after the collision.

After the collision, the dispersive tails (enlarged in Fig. 5) show that the GN equations more accurately approximate the Euler equations than the Boussinesq equations. In fact, the GN equations does a remarkable job at capturing both the phase and amplitude of the small trailing waves.

After the collision, both waves are retarded from their own pathlines. This phase shift is the salient feature of the nonlinear interaction. The decay of kinetic energy by the retardation upon merging is compensated for by the increase of potential energy, or the increase of the peak height (Wu 1995). For the weakly nonlinear collision, the phase shift of one wave is known to be proportional to the square root of amplitude of the

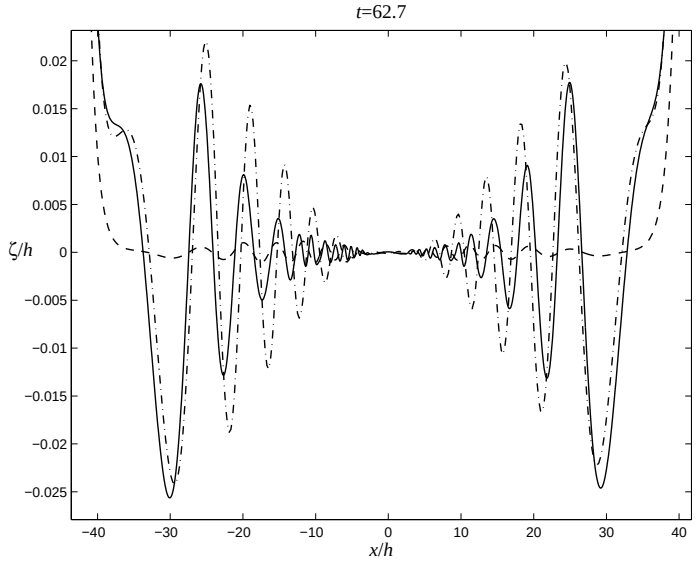

Figure 8: The trailing tails after the head-on collision shown in Fig. 7 at $t = 62.7$ for the Euler (solid curve), GN (dash-dotted curve) and Boussinesq (dashed curve) equations. The GN solution is remarkably close to the Euler solution.

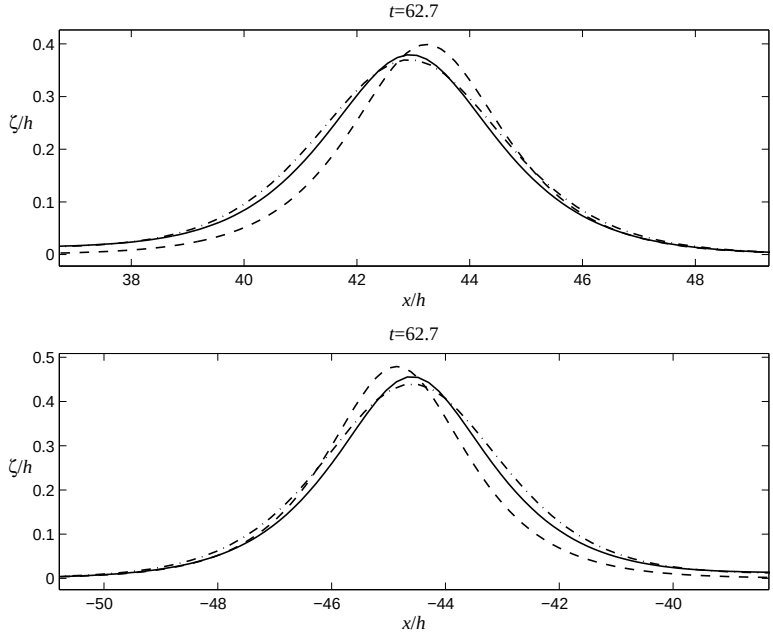

Figure 9: The wave profiles for $F = 1.172$ and $F = 1.201$ after the head-on collision shown in Fig. 7 for the Euler (solid curve), GN (dash-dotted curve) and Boussinesq (dashed curve) equations. The Boussinesq wave is a poor approximation to the Euler wave after the collision.

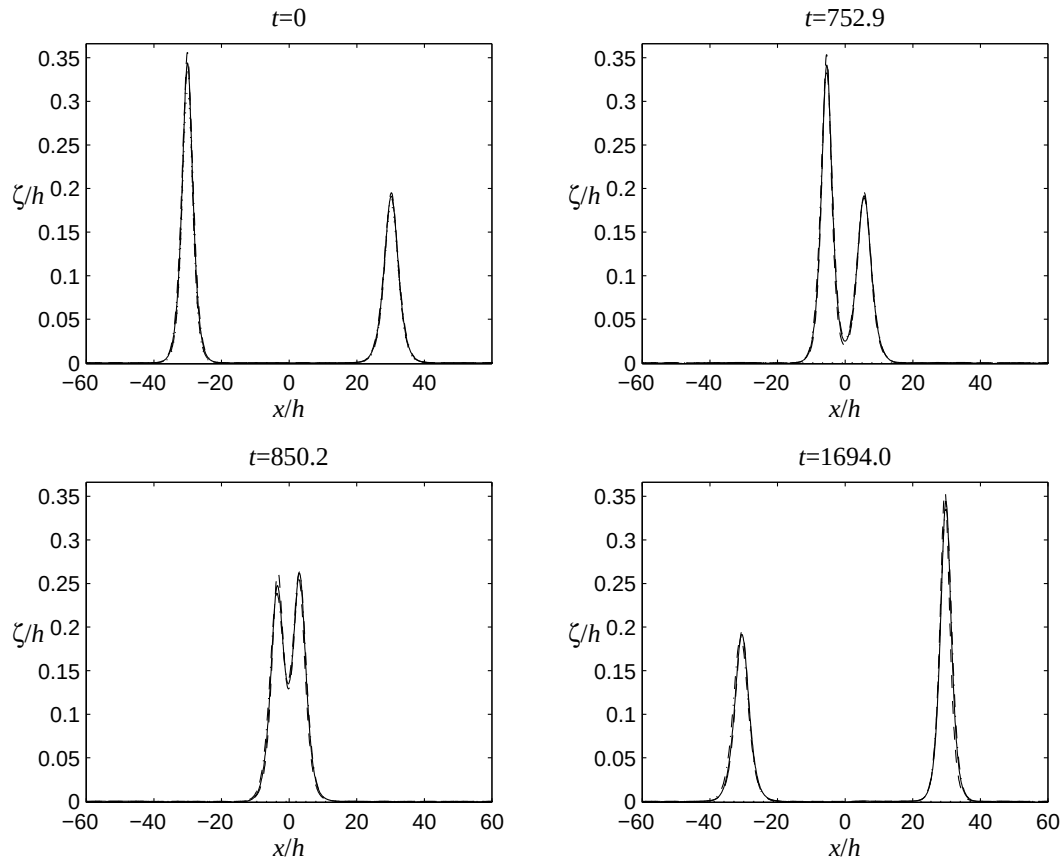

Figure 10: Overtaking collision of two solitary waves of the Euler (solid curve), the GN (dash-dotted curve), the Boussinesq (dashed curve) and the KdV equations (dotted curve), respectively, with $F = 1.156$ and $F = 1.0904$. The calculation is shown in a moving frame corresponding to $F = 1.123$. Unlike the head-on collision, the two peaks never merge into a single humped pulse and the emerging solitary waves are very close to the incident waves.

other wave. That is $\Delta x/h = (\text{amplitude}/3)^{1/2}$ (Wu 1995). This phase shift is too small to be accurately measured in our numerical solutions, but the finite amplitude effect on the phase shift can be identified from the relative positions of different solitary waves. The weakly nonlinear model (Boussinesq equations) underpredicts the phase shift after the collision, while the phase shift in the GN equations is very close to that in the Euler equations (Fig. 6).

The phase shift is more noticeable in collisions of higher amplitude waves with $F = 1.172$ and $F = 1.201$ as shown in Figs. 7, 8 and 9. The differences between the dispersive

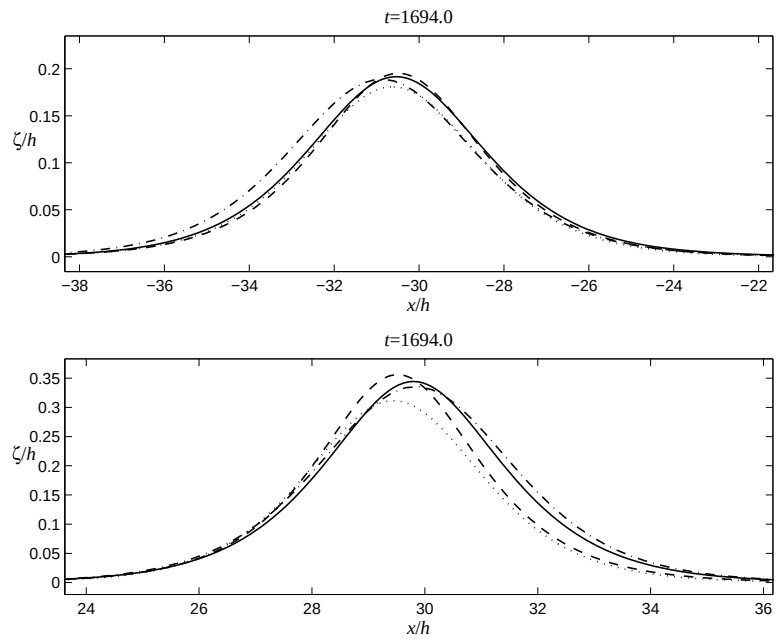

Figure 11: Comparison of solitary wave profiles with $F = 1.156$ and $F = 1.0904$ after the overtaking collision, shown in Fig. 10; Euler (solid curve), GN (dash-dotted curve), Boussinesq (dashed curve) and the KdV equations (dotted curve).

tails and phase shifts in this highly nonlinear regime are even more dramatic. The strong nonlinearity in the GN and Euler equations induces the larger phase shift.

The head-on collisions verify that solitary waves of these three systems are not true solitons, *i.e.* they do not maintain the same shape after interactions, and dispersive tails become larger as solitary wave amplitudes increase.

5.2 Overtaking collision

Figure 10 shows the overtaking collision between two solitary waves with the Froude numbers of $F = 1.156$ and $F = 1.09$ in a frame moving with the speed $F = 1.123$. Initially, the amplitudes of the larger waves are $A_K/h = 0.3114$, $A_E/h = 0.3441$, $A_G/h = 0.3356$ and $A_B/h = 0.3561$, and the amplitude of the smaller waves are $a_k/h = 0.1808$, $a_e/h = 0.1911$, $a_g/h = 0.1889$ and $a_b/h = 0.1952$ for the KdV, Euler, GN and Boussinesq equations, respectively.

Unlike the head-on collision case, after an overtaking collision, waves are almost elastic

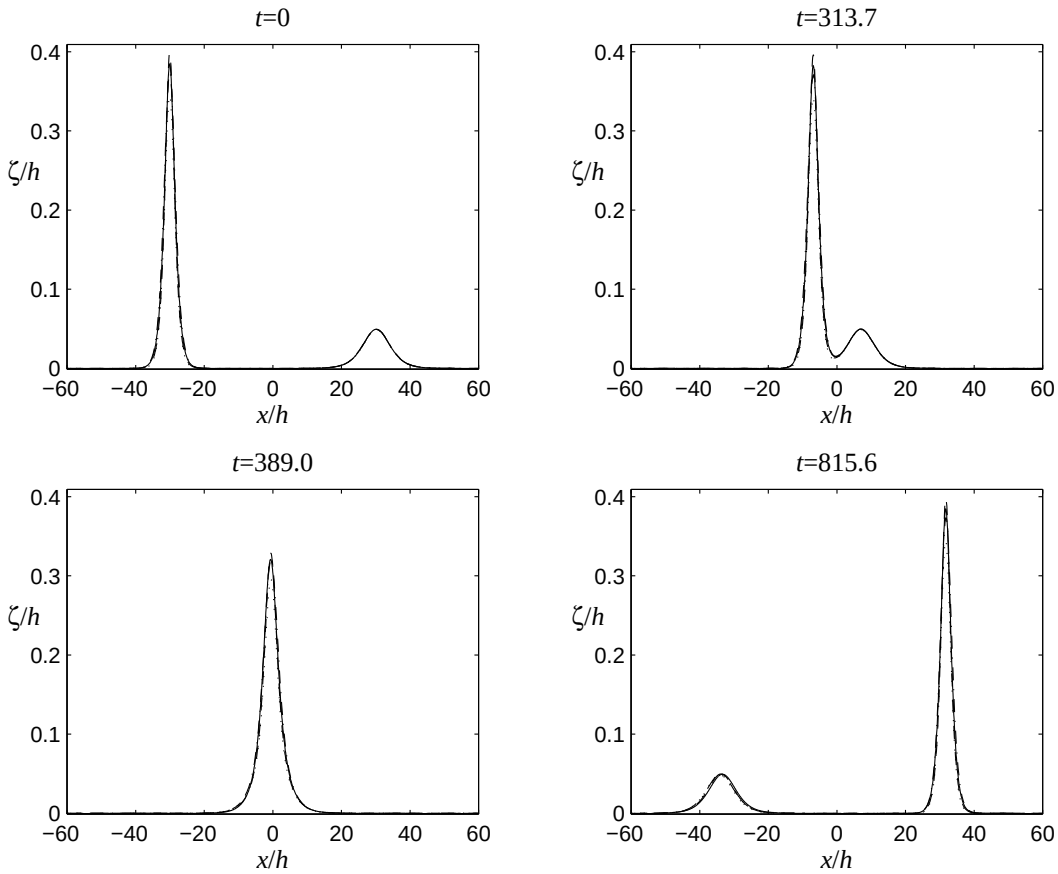

Figure 12: When a very fast wave overtakes a slow wave, the slower wave is 'swallowed' by the fast wave creating a single pulse wider and lower than the fast wave. The solutions of the Euler (solid curve), the GN (dash-dotted curve), the Boussinesq (dashed curve) and the KdV equations (dotted curve) with the Froude numbers $F = 1.172$ and $F = 1.024$ are all in close agreement. The solutions are shown moving in a reference frame corresponding to $F = 1.098$.

and the emerging solitary waves are almost identical to the incident waves. The KdV solitons collisions are always perfectly elastic.

When one solitary wave overtakes another one of similar height, as in Fig. 10, the waves never merge into a single peak. There is always a gap between their peaks and their amplitudes gradually change in time; the larger amplitude of the faster wave decreases while the smaller amplitude of the leading wave increases. This phenomenon was explained earlier by Wu (1995) for the Boussinesq equations. He showed that when the ratio of the amplitude of two waves is less than three, then the Boussinesq waves do not form a single

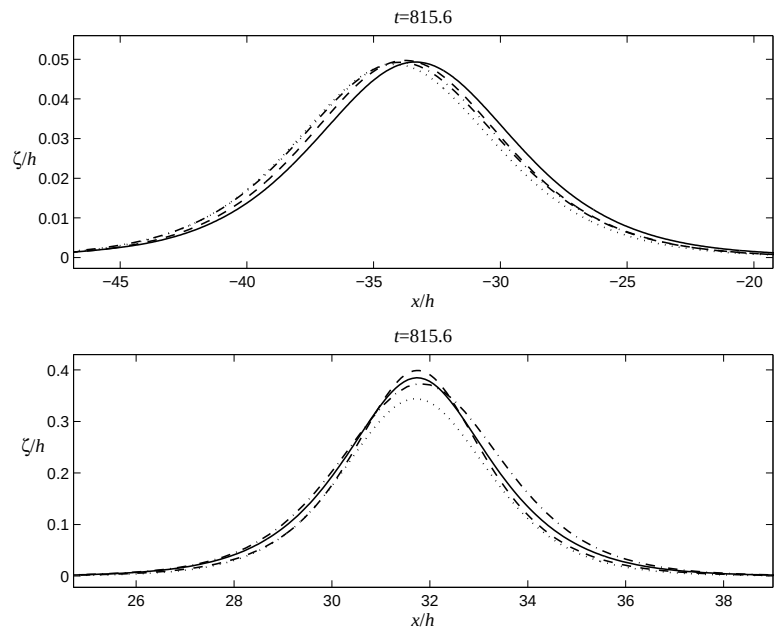

Figure 13: The solitary wave profiles of the Froude numbers $F = 1.172$ and $F = 1.024$ after the overtaking collision shown in Fig. 12; Euler (solid curve), GN (dash-dotted curve), Boussinesq (dashed curve) and the KdV equations (dotted curve), respectively. Notice that the position of the fast waves are all close, but the Euler slow wave is ahead of the other slow waves.

peak in an overtaking collision. Above this ratio, when a solitary wave overtakes another, they merge together to form a single peak. The amplitude ratio in the simulation shown in Fig. 10 is less than 3 and two solitary waves never merge.

A large solitary wave overtaking a smaller one experiences a forward phase shift, while the smaller one shifted a backward (Whitham, 1974). The height at the center of mass is known to depend on the difference of two wave amplitudes. Fig. 11 shows that in a collision the larger waves of the GN and Euler equations have a larger phase shift and move slightly more forward than those of the weakly nonlinear models. The smaller waves of all models have almost the same phase shift.

In Fig. 12, we show two solitary-wave interactions with the Froude numbers $F = 1.172$ and $F = 1.024$. The simulation was performed in a frame moving with the speed corresponding to $F = 1.098$. The amplitude ratio of the incident waves is about 7.8. In this case the larger wave merges with the smaller wave to form a single peak during the

interaction. The amplitude of the merged peak is about $A_E/h = 0.3208$. This is smaller than the amplitude of the larger wave, $A_E/h = 0.3847$, as the weakly nonlinear theory predicts.

Fig. 13 illustrates that the solitary waves of all these models are almost in phase after an overtaking collision. During the collision, the smaller solitary wave of the Euler equations is shifted back less than the approximate models and is slightly ahead of them.

In our numerical experiments, we observed that although the solitary waves of the four systems have slightly different phase shifts after an overtaking collision, all three model equations were good approximations of the Euler equations.

6 Conclusion

The full Euler equations for free surface problems are difficult to solve because they are highly nonlinear and the domain boundary changes to follow the surface waves. The numerical solution of these surface waves in our new exact one-dimensional evolution equations (2.4) is much easier than other approaches, such as the boundary integral method. The relative error of the conserved mass, horizontal momentum and energy was below 0.43% in the extremely long simulations until dimensionless time $t = 1700$ shown in Fig. 11. Although in these comparisons, we only considered solitary waves, the equations (2.4) for surface gravity-capillary waves are valid for periodic waves of arbitrary wavelength.

We demonstrated that the head-on collision of large (nonlinear) waves can be captured only by the strongly nonlinear models such as the GN equations. Steady solitary wave solutions of the Euler equations are well approximated by the weakly nonlinear Boussinesq equations, but when the waves collide, the Boussinesq dynamics are quite different from strongly nonlinear models such as the GN or Euler equations.

We observed that the GN equations were a better approximation of the Euler equations in the nonlinear regime. This is expected since the GN equations are a higher-order nonlinear approximation to the Euler equations than the other weakly nonlinear models.

We conclude that the GN equations are valid for a wider range of solutions than any of the weakly nonlinear asymptotic models we considered. Thus the GN equations would be more appropriate when simulating more realistic physical problems such as coastal waves with uneven bottom topography.

This work was supported by the US Department of Energy. We would like to thank R. Camassa for his helpful suggestions.

References

[1] C. J. Amick and J. F. Toland, *On periodic water-waves and their convergence to solitary waves in the long-wave limit*, Phil. Trans. Royal Soc. London A **303** (1981), 633–669.

[2] C. J. Amick and J. F. Toland, *On solitary water-waves of finite amplitude*, Arch. Rational Mech. Anal. **76** (1981), 9–95.

[3] T. Beale, *The existence of solitary waves*, Comm. Pure Appl. Math **30** (1977), 373–389.

[4] T. B. Benjamin and P. J. Olver, *Hamiltonian structure, symmetries and conservation laws for water waves*, J. Fluid Mech **125** (1982), 137–185.

[5] J. Boussinesq, *Essai sur la théorie des eaux courants*, Mem. prés. div. Sav. Acad. Sci. Inst. Fr. **23** (1877), 1–680.

[6] W. Choi, *Nonlinear evolution equation for two-dimensional surface waves in a fluid of finite depth*, J. Fluid Mech **295** (1995), 381–394.

[7] W. Choi and R. Camassa, *Fully nonlinear internal waves in a two-fluid system*, J. Fluid Mech **396** (1999*a*), 1–36.

[8] W. Choi and R. Camassa, *Exact evolution equations for surface waves*, J. Eng. Mech **125** (1999*b*), 756–760.

[9] A. L. Dyachenko, V. E. Zakharov, and E. A. Kuznetsov, *Nonlinear dynamics of the free surface of an ideal fluid*, Plasma Physics Report **22** (1996), 916–928.

[10] J. D. Fenton and M. M. Rienecker, *A Fourier method for solving nonlinear water-wave problems: application to solitary-wave interactions*, J. Fluid Mech **118** (1982), 411–443.

[11] K. O. Friedrichs and D. H. Hyers, *The existence of solitary waves*, Comm. Pure Appl. Math. **7** (1954), 517–550.

[12] A. E. Green and P. M. Naughdi, *Derivation of equations for wave propagation in water of variable depth*, J. Fluid Mech **78** (1976), 237–246.

[13] D. J. Korteweg and G. de Vries, *On the change of form of long waves advancing in a rectangular canal, and on a new type of long stationary waves*, Phil. Mag **39** (1895), 422–443.

[14] M. S. Longuet-Higgins, *On the mass, momentum, energy and circulation of a solitary wave*, Proc. R. Soc. Lond **A. 337** (1974), 1–13.

[15] M. S. Longuet-Higgins and E. .D. Cokelet, *The deformation of steep surface waves on water I. A numerical method of computation*, Proc. R. Soc. Lond **A. 350** (1976), 1–26.

[16] M. S. Longuet-Higgins and J. D. Fentons, *On the mass, momentum, energy and circulation of a solitary wave. II*, Proc. R. Soc. Lond **A. 340** (1974), 471–493.

[17] W. E. Schiesser, *Computational mathematics in engineering and applied science: ODEs, DAEs, and PDEs*, CRC Press, (1993).

[18] A. C. Scott, F. Y. F. Chu, and D. W. McLaughlin, *The soliton: a new concept in applied science*, Proc. IEEE **61** (1973), 1443–1483.

[19] M. Staley, *DFTmod, modules for discrete Fourier transforms and filters*, Technical report, the Los Alamos National Laboratory, 1999.

[20] G. Wei, J. T. Kirby, S. T. Grilli, and R. Subramanya, *A fully nonlinear Boussinesq Model for surface waves. 1. Highly nonlinear unsteady waves*, J. Fluid Mech. **294** (1995), 71–92.

[21] G. B. Whitham, *Linear and nonlinear waves*, John Wiley and Sons, 1974.

[22] T. Y. Wu, *Bidirectional soliton street*, Acta Mechanica Sinica **11** (1995), 289–306.